

An efficient wavelet-based physics-informed neural networks for singularly perturbed problems

Himanshu Pandey¹, Anshima Singh² and Ratikanta Behera³

Department of Computational and Data Sciences, Indian Institute of Science, Bangalore, India

E-mail,¹: phimanshu@iisc.ac.in

E-mail,²: anshimasingh@iisc.ac.in

E-mail,³: ratikanta@iisc.ac.in

Abstract. Physics-informed neural networks (PINNs) are a class of deep learning models that utilize physics in the form of differential equations to address complex problems, including ones that may involve limited data availability. However, tackling solutions of differential equations with rapid oscillations, steep gradients, or singular behavior becomes challenging for PINNs. Considering these challenges, we designed an efficient wavelet-based PINNs (W-PINNs) model to address this class of differential equations. Here, we represent the solution in wavelet space using a family of smooth-compactly supported wavelets. This framework represents the solution of a differential equation with significantly fewer degrees of freedom while still retaining the dynamics of complex physical phenomena. The architecture allows the training process to search for a solution within the wavelet space, making the process faster and more accurate. Further, the proposed model does not rely on automatic differentiations for derivatives involved in differential equations and does not require any prior information regarding the behavior of the solution, such as the location of abrupt features. Thus, through a strategic fusion of wavelets with PINNs, W-PINNs excel at capturing localized nonlinear information, making them well-suited for problems showing abrupt behavior in certain regions, such as singularly perturbed and multiscale problems. The efficiency and accuracy of the proposed neural network model are demonstrated in various 1D and 2D test problems, i.e., the FitzHugh-Nagumo (FHN) model, the Helmholtz equation, the Maxwell equation, and the Allen-Cahn equation, along with other highly singularly perturbed nonlinear differential equations. The proposed model significantly improves with traditional PINNs, recently developed wavelet-based PINNs, and other state-of-the-art methods.

AMS subject classifications: 65L11, 68T07, 65T60

Key words: Physics-informed neural networks, Wavelets, Singularly perturbed problems, Multiscale problems

1. Introduction

Singularly perturbed problems (SPP.s) can be described using differential equations featuring at least one small parameter, popularly known as the “perturbation parameter(s)”. Specifically, when the parameter is very small (close to zero), the solution exhibits thin transition layers, often adjacent to the boundaries of the domain of interest. Consequently, the solution or its derivatives undergo rapid fluctuations within specific domain areas while maintaining smooth behavior outside these regions [1]. These problems are encountered in various physical systems that simultaneously contain both slow and fast varying components in the fields of science and engineering such as fluid dynamics [2], chemical reactors [3], financial modeling [4], modeling of semiconductor devices [5], and convective heat transfer problems with high Péclet numbers [6].

The numerical solutions of these parameter-dependent problems based on the discretization approaches are impractical since it is affected by the parameter. Further, a large number of mesh points are required to produce sufficiently precise approximations of the actual solution for various perturbation parameter values. Many methods have been developed to address this challenge, such as parameter-uniform, parameter-robust, or uniformly convergent approaches like Fitted Operator Methods (FOMs)

[7, 8] and Fitted Mesh Methods (FMMs) [9, 10]. Moreover, to address the challenges with meshes, various meshfree methods, such as the moving least squares (MLS) method [11], element-free Galerkin approach [12], and the local Petrov–Galerkin method [13], have been developed to solve SPPs numerically.

This study concentrates on one such class of methods, which not only eliminates meshes but also has the ability to handle complex geometry and higher-dimensional problems, namely, physics-informed neural networks (PINNs). A few of the earliest works on solving differential equations utilizing neural networks were presented by Dissanayake *et al.* [14] and Lagaris *et al.* [15]. Their method required a trial solution that satisfies all boundaries and initial conditions. However, this technique often fails if a problem has complex behavior, and finding appropriate trial solutions for such problems becomes challenging. Later, Raissi *et al.* [16] introduced PINNs, which incorporate initial and boundary conditions into the network’s loss function without considering a trial solution beforehand. Following this work, different types of PINNs, such as variational physics-informed neural networks (VPINN) [17], gradient-enhanced physics-informed neural networks (GPINN) [18], and extended physics-informed neural networks (XPINN) [19] and many other have been developed to enhance the performance of conventional PINN. For more details, see a comprehensive review of PINNs [20, 21] and references therein.

Despite many significant advantages, PINNs encounter challenges in accurately handling equations with sharp gradients or rapid oscillations [21]. This difficulty arises because the various components in the loss function have varying convergence rates during training. PINNs need to efficiently represent and learn these features that vary significantly across various scales. While existing theories address issues related to isolated rapid changes, using techniques like domain splitting [22, 23] or using trainable weights to balance loss terms dynamically [24], these approaches can be cumbersome to implement. Furthermore, the authors of [25] introduced an improved physics-informed neural networks algorithm, which involved some modifications from the approach described in [22]. A singularity term was included in the calculation formula to account for the singularity of the equation. Other approaches [26, 27] in which authors sampled dense training points near high-gradient regions to improve convergence. Motivated by the reviewed research and identified shortcomings, this work proposes a novel modified version of PINNs *i.e.*, wavelet-based physics-informed neural networks (W-PINNs), which exploit the ability of wavelets to address these challenges.

The localization properties of wavelets make them beneficial when analyzing problems with localized features, such as initial or boundary layers, in SPPs [28, 29]. Mallat’s work [30] and Daubechies’ contributions [31] lay down the foundational principles of wavelet analysis. Wavelets excel at capturing nonlinear information within localized regions of the solution [32, 33]. In contrast, neural networks are well-known for learning and modeling global nonlinear relationships. By incorporating wavelets with neural networks, we can potentially leverage the ability of wavelets to extract these localized nonlinearities. This can complement the neural network’s nonlinear learning capability and potentially enhance the overall ability to capture intricate nonlinear patterns, possibly improving the accuracy of the network. The incorporation of wavelets into PINNs has been attempted in [34]. However, the authors of [34] focused on wavelets solely as activation functions, with the overall structure of PINNs remains unchanged from its original introduction. Our findings show that this method also fails to approximate SPPs satisfactorily.

In this study, we use the wavelet family to represent an approximate solution to the differential equation, and the weight of each family member is optimized using the W-PINN. Unlike previous neural network-based approaches, the proposed neural architecture does not rely on automatic differentiation for the derivatives involved in the loss function, which significantly reduces training time. Additionally, this method requires no prior information about the nature of the solution, making it practical and easy to implement. We use Gaussian and Mexican hat wavelets for implementation, and their performance is compared with conventional PINN and state-of-the-art methods to validate the efficacy. Our approach demonstrates high accuracy across a range of differential equations exhibiting steep gradients, rapid oscillations, singularities, and multiscale behavior, establishing it as a robust method for these classes of problems. The key contributions of this work can be summarized as follows:

- W-PINN introduces a framework that eliminates automatic differentiation in loss function derivative

computation, significantly accelerating training while maintaining or improving solution accuracy compared to recent methods in the literature.

- W-PINN effectively addresses the loss balancing challenges inherent in conventional PINNs, particularly for problems exhibiting multi-scale phenomena, singular behavior, or rapid oscillations in their solutions.
- The proposed method is validated through the FHN model, Helmholtz equation, Allen-Cahn equation, Maxwell equation, Lid-driven cavity flow, and various other singularly perturbed problems.

The organization of the remaining paper is outlined as follows: Section 2 initiates with the introduction of standard PINNs, followed by a thorough discussion on the design and operational mechanism of W-PINNs. Section 3 presents numerical results for various differential equations to demonstrate the effectiveness and accuracy of the proposed method. Finally, Section 4 serves as the concluding segment, offering a concise summary of the key findings, contributions, and future work along with limitations.

2. Methodology

2.1. Physics-informed neural networks (PINNs)

A neural network is a mathematical model consisting of layers of neurons interconnected via nonlinear operations. These layers include an input layer for initial data, multiple hidden layers for complex computations, and an output layer for predictions. It is widely acknowledged that with enough hidden layers and neurons per layer, a neural network can approximate any function [35]. The values of neurons in each layer depend on the previous layer in the following manner:

$$\begin{aligned} \text{Input layer: } \mathbf{z}^0 &= \mathbf{x} \in \mathbb{R}^{n_0}, \\ \text{Hidden layers: } \mathbf{z}^k &= \sigma(\boldsymbol{\omega}^k \mathbf{z}^{k-1} + \mathbf{b}^k), \quad 1 \leq k \leq L-1, \\ \text{Output layer: } \mathbf{z}^L &= \boldsymbol{\omega}^L \mathbf{z}^{L-1} + \mathbf{b}^L \in \mathbb{R}^{n_L}, \end{aligned} \quad (1)$$

where $\mathbf{z}^k \in \mathbb{R}^{n_k}$ is the outcome of k -th layer, $\boldsymbol{\omega}^k \in \mathbb{R}^{n_k \times n_{k-1}}$, $\mathbf{b}^k \in \mathbb{R}^{n_k}$, and n_k is the number of neurons in k^{th} layer. Here, $\boldsymbol{\omega}$ and \mathbf{b} denote the weight and bias, the model parameters to be optimized. Moreover, σ is a nonlinear mapping known as an activation function. This process is widely known as feed-forward propagation. We define a loss function (\mathcal{L}) for network output, which quantifies the disparity between the network's predictions and the desired outcomes. The neural network is trained using backpropagation [36], a technique wherein optimization algorithms, such as gradient descent, to minimize loss function and fine-tune the model parameters ($\boldsymbol{\omega}, \mathbf{b}$). Trained parameters capture the underlying structure of the problem in consideration. A well-known class of neural network is physics-informed neural networks (PINNs), which incorporate the underlying physics of the system by using a governing set of equations along with initial and boundary conditions into the loss function. It measures how much the network's predicted solution violates the differential equation at several collocation points. Mathematically, it can be written as $\mathcal{L} = \mathcal{L}_{\text{res}} + \mathcal{L}_{\text{ic}} + \mathcal{L}_{\text{bc}}$, where \mathcal{L}_{res} denotes the residual mean squared error, \mathcal{L}_{ic} and \mathcal{L}_{bc} denote mean squared errors for initial and boundary conditions respectively. During optimization, the derivative of the loss function with respect to the model parameters and derivatives of the network's output with respect to input parameters, exhibited in the loss function are required. These derivatives are effectively computed using "automatic differentiation" [37]. Thus, the objective of PINNs is to identify the optimal parameters that minimize the specified loss function, which encapsulates all physics-related information.

2.2. Wavelet-based physics-informed neural networks (W-PINNs)

PINNs have emerged as a promising mesh-free approach for solving wide varieties of differential equations. However, their performance significantly deteriorates when dealing with problems exhibiting high

gradients, rapid oscillations or singular behavior, primarily due to challenges in balancing different loss terms and accurately computing derivatives through automatic differentiation. Recent literature has proposed several approaches to address these limitations. McClenny *et al.* introduced Self-adaptive PINNs (SA-PINNs)[24] that employ trainable weights to balance loss terms dynamically, while Wang *et al.* (2024) developed a practical PINN framework for multi-scale problems with multi-magnitude loss terms (MMPINN)[23] framework incorporating specialized architectures and regularization strategies for multi-scale problems. While these methods demonstrate improved performance, they still face computational overhead from automatic differentiation and require careful tuning of multiple hyperparameters. The proposed wavelet-based PINN (W-PINN) framework offers an elegant solution to these challenges by expressing the solution as a linear combination of wavelet basis functions. By training the coefficients rather than the solution directly, W-PINN eliminates the need for automatic differentiation in computing derivatives in loss function, as they can be obtained analytically from the wavelet basis functions. This approach not only significantly reduces computational cost but also naturally handles multi-scale features and balances different loss terms.

Formulation of W-PINN starts with a family of wavelets, whose members are dilates and translates of the mother wavelet. The dilated and translated version of the mother wavelet function, $\psi(x)$ for $j, k \in \mathbb{Z}$ can be written as

$$\Psi_{j,k}(x) = \sqrt{2^j} \psi(2^j x - k),$$

here j is the exponent of dilation, and k is the translation parameter. In order to define the number of family members, we fix the set of resolution for the family as J . For a given j in J , translation parameter k ranges from $\lceil a \cdot 2^{j+1} \rceil$ to $\lceil b \cdot 2^{j+1} \rceil$, where $\lceil \cdot \rceil$ is a ceiling function. This way of constructing a family enables to cover the whole domain, $[a, b]$ with various resolutions. After constructing a family of wavelets, we approximate the solution of the differential equation as:

$$\hat{u}(x) = \sum_{j=J_1}^{J_N} \sum_{k=\lceil a \cdot 2^{j+1} \rceil}^{\lceil b \cdot 2^{j+1} \rceil} c_{j,k} \Psi_{j,k}(x) + \mathcal{B}, \quad (2)$$

where \mathcal{B} is bias, J_i is i^{th} resolution and N is the total number of resolutions in set J . Extension of this formulation for higher dimensional problem is straight forward, for instance here is formulation for a 2D problem:

$$\Psi_{j_1, j_2, k_1, k_2}(x, y) = \sqrt{2^{j_1} \cdot 2^{j_2}} \psi_X(2^{j_1} x - k_1) \psi_Y(2^{j_2} y - k_2), \quad (3)$$

$$\hat{u}(x, y) = \sum_{j_1=J_{11}}^{J_{1N_1}} \sum_{j_2=J_{21}}^{J_{2N_2}} \sum_{k_1=\lceil a_1 \cdot 2^{j_1+1} \rceil}^{\lceil b_1 \cdot 2^{j_1+1} \rceil} \sum_{k_2=\lceil a_2 \cdot 2^{j_2+1} \rceil}^{\lceil b_2 \cdot 2^{j_2+1} \rceil} c_{j_1, j_2, k_1, k_2} \Psi_{j_1, j_2, k_1, k_2}(x, y) + \mathcal{B}, \quad (4)$$

where the domain $\Omega = [a_1, b_1] \times [a_2, b_2]$ is discretized using resolution parameters J_1 and J_2 corresponding to the x and y dimensions respectively. The translation parameters k_1 and k_2 define the positioning of basis functions along these respective dimensions. This hierarchical construction of wavelet families at different resolutions enables capturing solution features at multiple scales - from broad, global behavior to fine, local details. In this study, we consider two mother wavelets, namely, the Gaussian and the Mexican Hat, which are single and double derivatives of the Gaussian function, respectively. The mathematical expressions for the Mexican hat ($\psi^M(x)$), Gaussian ($\psi^G(x)$) can be written as

$$\psi^M(x) = (1 - x^2)e^{-\frac{x^2}{2}}, \quad \psi^G(x) = -xe^{-\frac{x^2}{2}}.$$

In equations (2) and (4), we added a bias \mathcal{B} to make a degree of freedom in approximating solutions with non-zero means, as the Mexican Hat and Gaussian are symmetrical wavelets.

We employ W-PINN to obtain an approximate solution, as described above. W-PINN is composed of two parts: a trainable network that predicts coefficients by forming a fully connected network, and a

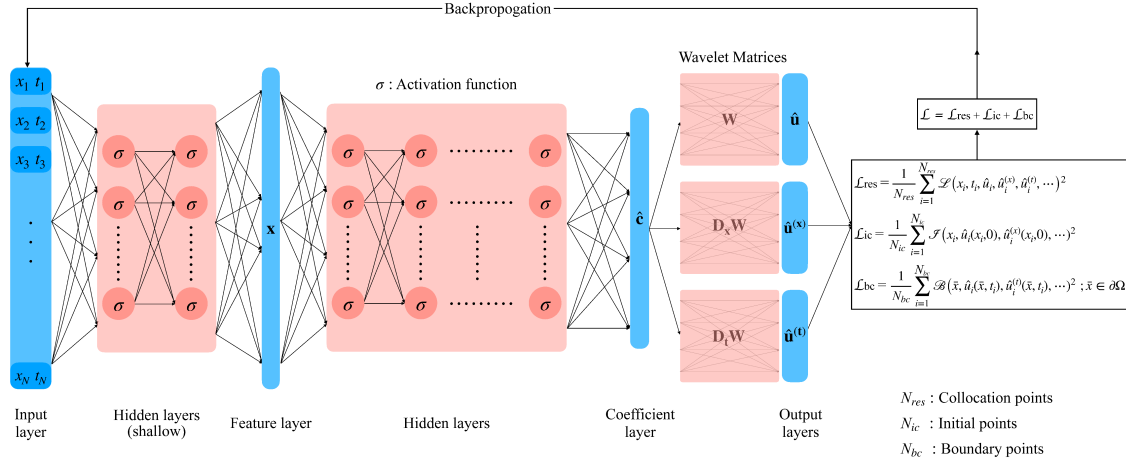


Figure 1: A W-PINN architecture.

non-trainable network that constructs the final solution and its derivatives using these coefficients and pre-computed wavelet matrices. This formulation eliminates the need for automatic differentiation (AD) in computing PDE residuals. While AD provides machine-precision derivatives, but it comes at cost of maintaining computation-intensive computational graphs that grow increasingly complex with network depth and order of derivatives involved. Our wavelet-based approach not only makes training faster by eliminating need of computational graph but also avoid potential numerical instabilities that commonly arise in AD during training, particularly in problems exhibiting high gradients or singular behavior. This approach aligns with recent developments in the field, such as DT-PINN [38], which achieved two to four times speedups over AD-based PINNs by eliminating AD through meshless radial basis function-finite differences (RBF-FD). However, our wavelet-based formulation provides the additional advantage of naturally handling multi-scale features through its hierarchical basis structure. The architecture of W-PINN for a two-dimensional problem is illustrated in Figure 1. In general, for a d -dimensional problem, the network architecture comprises an input layer with d neurons corresponding to the spatial-temporal dimensions. These inputs are processed through a shallow network that maps each collocation point to a corresponding entry in the feature layer. For one-dimensional problems, this mapping can be simplified by directly using the input layer as the feature layer. Now, the feature layer passes through a fully connected network to get coefficients. To further enhance model performance, these coefficients can be separately fine-tuned through hyperparameter optimization. The final solution is then computed by combining these optimized coefficients with the pre-calculated wavelet matrices. Once we have an approximate solution and its derivatives, we get the loss function of the network using the mean square of residuals and the mean square error of the initial and boundary conditions. W-PINN requires collocation points spanning all over the domain as a training set and a wavelet matrix and its derivative matrices up to the order of the differential equation in consideration. These wavelet matrices serve as the weights of the non-trainable network. A trainable bias is also added to the wavelet matrix (\mathbf{W}) in order to incorporate \mathcal{B} . For a given set of collocation points $\mathbf{x} = (x_0, x_1, \dots, x_N)$, the wavelet matrices are constructed as follows:

$$\mathbf{W} = \begin{pmatrix} \psi_{0,0}(x_0) & \cdots & \psi_{j,k}(x_0) & \cdots & \psi_{J-1,2^{J-1}-1}(x_0) \\ \psi_{0,0}(x_1) & \cdots & \psi_{j,k}(x_1) & \cdots & \psi_{J-1,2^{J-1}-1}(x_1) \\ \vdots & \vdots & \vdots & \vdots & \vdots \\ \psi_{0,0}(x_N) & \cdots & \psi_{j,k}(x_N) & \cdots & \psi_{J-1,2^{J-1}-1}(x_N) \end{pmatrix}, \mathbf{D}_1 \mathbf{W} = \begin{pmatrix} \psi'_{0,0}(x_0) & \cdots & \psi'_{j,k}(x_0) & \cdots & \psi'_{J-1,2^{J-1}-1}(x_0) \\ \psi'_{0,0}(x_1) & \cdots & \psi'_{j,k}(x_1) & \cdots & \psi'_{J-1,2^{J-1}-1}(x_1) \\ \vdots & \vdots & \vdots & \vdots & \vdots \\ \psi'_{0,0}(x_N) & \cdots & \psi'_{j,k}(x_N) & \cdots & \psi'_{J-1,2^{J-1}-1}(x_N) \end{pmatrix},$$

where $\psi'(x)$ is single derivate of $\psi(x)$ and similarly $\mathbf{D}_2 \mathbf{W}$ is constructed by double derivative of $\psi(x)$.

3. Results and discussions

In this section, we present the results obtained using the proposed method over a handful of examples and compare them with the performance of conventional PINNs and state-of-the-art methods. For a fair comparison, all network parameters are kept the same throughout and are tabulated along with the examples. We utilize the Adam optimizer [39], which combines two stochastic gradient descent algorithms: gradient descent with momentum and root mean squared propagation (RMSProp). RMSprop, also known as adaptive gradient descent, adapts the learning rate with iterations. Adam optimizer is memory efficient and is well suited for problems with high-dimensional parameter spaces.

The trainable parameters of networks are initialized using Xavier’s technique or Glorot initialization [40], which, in contrast to random initialization, initializes parameters in a suitable range to achieve faster convergence during training. During backpropagation, it maintains gradients within a reasonable range (not too low or high), thereby preventing the algorithm from getting stuck in poor local minima. Besides this, it can also reduce the need for extensive hyperparameter tuning, particularly the learning rate. We sampled the training set by Sobol sequencing throughout the domain as we need efficient exploration of the entire input space for a single training set. For evaluation purposes, we employ the relative L_2 metric over uniform samples across the domain.

$$\text{Relative } L_2 \text{ error} = \sqrt{\frac{\sum_{i=1}^M (u_i - \hat{u}_i)^2}{\sum_{i=1}^M u_i^2}}, \quad (5)$$

where M represents the total number of testing samples, u_i is the exact solution and \hat{u}_i is the predicted one for the i^{th} sample. In the case of problems with unknown solutions, we consider the exact solution as a numerical solution obtained from the Scipy solver.

For implementation purposes, the PyTorch 2.4.1 with CUDA 12.1 is used. Training is done on the NVIDIA RTX A6000, which has 48GB of GPU memory. As the performance of a neural network is highly sensitive to the initialization of its parameters, so we perform each experiment five times and report relative L_2 -error and average training time based on these five random runs.

Example 1. Consider the following one-dimension linear advection-diffusion equations [41]:

$$\begin{cases} \epsilon \frac{d^2 u}{dx^2} + (1 + \epsilon) \frac{du}{dx} + u = 0, & x \in (0, 1), \\ u(0) = 0, & u(1) = 1. \end{cases} \quad (6)$$

Here, $0 < \epsilon \ll 1$. The exact solution to the considered problem is

$$u(x) = \frac{\exp(-x) - \exp(-\frac{x}{\epsilon})}{\exp(-1) - \exp(-\frac{1}{\epsilon})}.$$

Table 1: Parameters used for Example 1.

| Parameters | Value |
|----------------------------------|-----------------|
| Set of resolutions (J_M/J_G) | [0,8]/[0,9] |
| Number of hidden layers | 6 |
| Neurons per layer | 100 |
| Number of collocation points | 10^3 |
| Maximum number of iterations | 2×10^4 |

Table 2: Training time (in seconds) of PINN and W-PINN with network depth for Example 1.

| Depth | PINN | W-PINN |
|-------|-------|--------|
| 2 | 58.3 | 21.4 |
| 4 | 80.1 | 26.2 |
| 8 | 131.3 | 33.4 |
| 16 | 223.4 | 41.7 |
| 32 | 367.1 | 58.8 |

Table 3: Performance comparison of various methods for Example 1.

| ϵ | Method | L_2 -error | Average Training Time |
|----------------------|-------------------------|--------------|-----------------------|
| $\epsilon = 2^{-4}$ | PINN | 7.9e-05 | 1m 58s |
| | Wavelet Activation [34] | 3.9e-05 | 52s |
| | W-PINN (Gaussian) | 2.5e-05 | 23s |
| | W-PINN (Mexican hat) | 8.1e-05 | 48s |
| $\epsilon = 2^{-7}$ | PINN | 0.83 | - |
| | Wavelet Activation [34] | 0.85 | - |
| | W-PINN (Gaussian) | 5.3e-04 | 18s |
| | W-PINN (Mexican hat) | 9.2e-04 | 23s |
| $\epsilon = 2^{-10}$ | PINN | 0.84 | - |
| | Wavelet Activation [34] | 0.85 | - |
| | W-PINN (Gaussian) | 3.1e-03 | 38s |
| | W-PINN (Mexican hat) | 4.2e-03 | 42s |

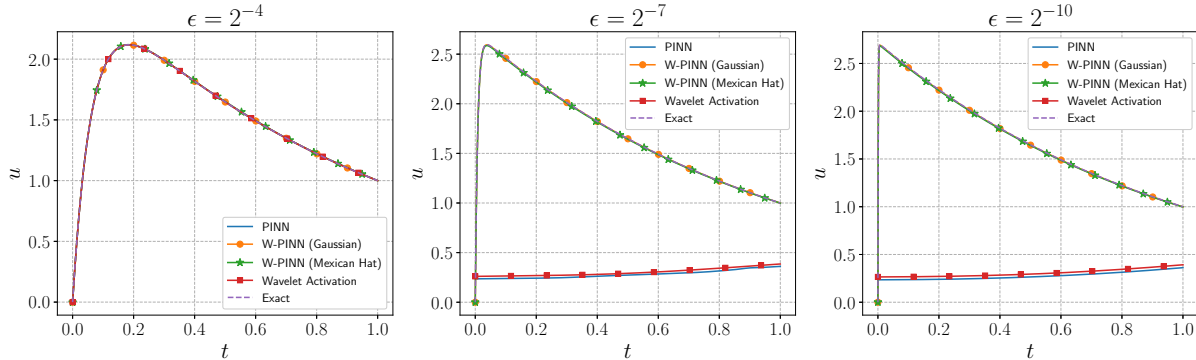


Figure 2: Comparison of solutions obtained by PINN, PINN with wavelet activation and W-PINN methods for Example 1.

Such models, called Friedrich’s boundary layer models, are often used to show how difficult it is to model viscous flow boundary layers [22]. It is impossible for PINNs to capture the singularity that happens when $\epsilon \rightarrow 0$.

The parameters of the W-PINN for the Example 1 are listed in Table 1. Table 2 compares the training time of automatic differentiation based PINN and W-PINN. The experiments were conducted with $\epsilon = 2^{-4}$ and each test was executed for 10^3 iterations. The results demonstrate that conventional PINN exhibits a steeper growth in training time with increase in network depth, requiring up to 6.2 times longer than W-PINN at depth 32. This substantial difference in computational overhead can be attributed to W-PINN’s elimination of automatic differentiation calculations, which become increasingly expensive in conventional PINNs as network depth increases. The comparison of various methods have been presented in Table 3, which provides the relative L_2 -error and average training time of the W-PINN, conventional PINN and PINN with gaussian-wavelet activation function [34]. This table shows the W-PINN approximates the solution with much smaller L_2 -error for lower values of ϵ . Similar observations are drawn from Figure 2, which demonstrate when $\epsilon = 2^{-4}$, there is no such sharp singularity near the origin,

all methods approximate the solution well. However, as ϵ decreases, the exact solution of the problem has a strong singularity near the origin. Then both PINN and PINN with wavelet activation function are unable to accurately capture the behavior of the solution, whereas W-PINN effectively resolves the singularity, with the predicted solution closely following the exact solution.

Example 2. Consider the following highly singularly perturbed non-linear problem [42]:

$$\begin{cases} \epsilon \frac{d^2 u}{dt^2} + (3+t) \frac{du}{dt} + u^2 - \sin(u) = f, & t \in (0, 1], \\ u(0) = 1, & u'(0) = 1/\epsilon, \end{cases} \quad (7)$$

where f is chosen such that $u(t) = 2 - \exp(-t/\epsilon) + t^2$ is the exact solution.

This example corresponds to a highly singularly perturbed non-linear equation with a known solution. For Example 2, the parameters of the network are given in Table 4. We compare the performance of W-PINN with the traditional PINN, and the PINN proposed in [34] (using Gaussian wavelet as an activation function) for various ϵ . The relative L_2 -error and average training time for these are tabulated in Table 5, which illustrates that the W-PINN outperforms other methods as it takes much less training time and provides better approximation, especially for lower values of ϵ . Figure 3 demonstrates similar

Table 4: Parameters used for Example 2.

| Parameters | Value |
|----------------------------------|-----------------|
| Set of resolutions (J_M/J_G) | [0,9]/[0,10] |
| Number of hidden layers | 8 |
| Neurons per layer | 200 |
| Number of collocation points | 10^4 |
| Maximum number of iterations | 2×10^4 |

Table 5: Performance comparison of various methods for Example 2.

| ϵ | Method | L_2 -error | Average Training Time |
|----------------------|-------------------------|--------------|-----------------------|
| $\epsilon = 2^{-4}$ | PINN | 1.2e-04 | 31s |
| | Wavelet Activation [34] | 2.1e-04 | 58s |
| | W-PINN (Gaussian) | 2.3e-04 | 48s |
| | W-PINN (Mexican hat) | 1.8e-04 | 51s |
| $\epsilon = 2^{-7}$ | PINN | 8.5e-02 | 1m 33s |
| | Wavelet Activation [34] | 2.2e-02 | 1m 14s |
| | W-PINN (Gaussian) | 1.3e-04 | 21s |
| | W-PINN (Mexican hat) | 3.7e-04 | 24s |
| $\epsilon = 2^{-10}$ | PINN | 1.4 | - |
| | Wavelet Activation [34] | 0.34 | - |
| | W-PINN (Gaussian) | 9.6e-05 | 27s |
| | W-PINN (Mexican hat) | 4.5e-04 | 48s |

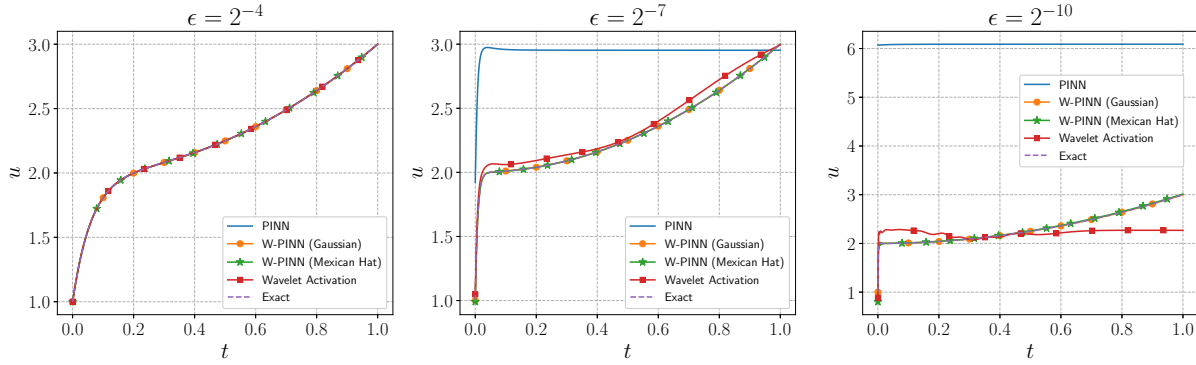


Figure 3: Comparison of solutions obtained by PINN, PINN with wavelet activation and W-PINN methods for Example 2.

observations, for $\epsilon = 2^{-10}$ both conventional PINN and PINN with the Gaussian wavelet as activation function [34] are unable to detect the singularity satisfactorily, whereas W-PINN effectively handles the singularity.

In addition, we investigate the relationship between the hyperparameters of W-PINN and its performance for this example. Figure 4 illustrates the relationship between the resolution level ($[0, J]$) and the relative L_2 -error. Here, we employ a network with 8 hidden layers, each containing 200 neurons, and fix 10,000 collocation points. It shows that W-PINN gives optimal results for a specific resolution range (not too high nor too low). Lower resolution is incapable of capturing sharp singularities, and a large J makes the loss function too complex to be optimized. The optimal range of the resolution is also dependent on the wavelet family. In this specific case, the W-PINN with Gaussian performed well for J , which is between 8 and 14, while this range is narrower for the Mexican hat. However, W-PINN performance also depends on the kind of wavelet used for a particular problem.

Figure 5 presents the effect of the number of collocation points on performance. We consider the identical network as previously used, with the Gaussian resolutions ($J_G = [0, 12]$) and the Mexican hat resolutions ($J_M = [0, 11]$). It is evident that the relative L_2 -error decreases as the number of collocation points increases. However, the error decrease is not significant beyond a certain threshold. After a certain number of collocation points, additional points do not come with any new information about the behavior of the problem in consideration.

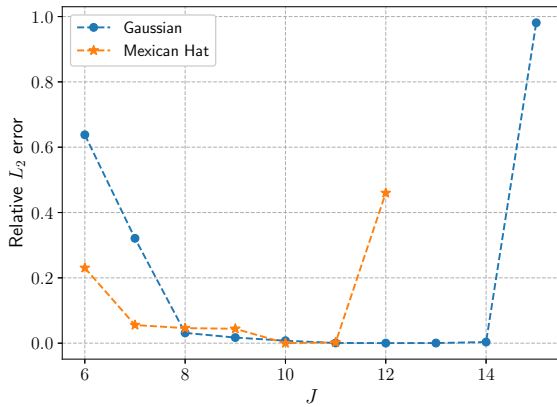


Figure 4: Relative L_2 -error variation with wavelet resolution levels ($[0, J]$) for Gaussian and Mexican Hat wavelets.

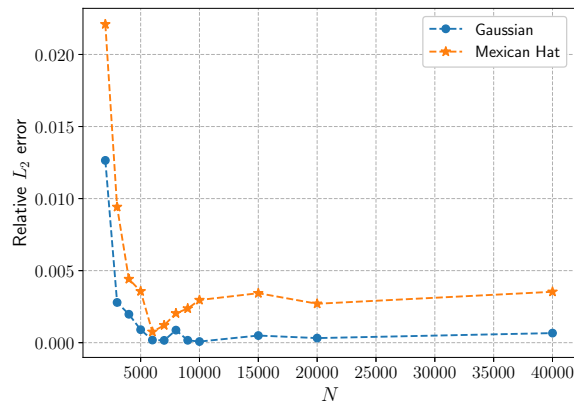


Figure 5: Relative L_2 -error variation with number of collocation points (N) for Gaussian and Mexican Hat wavelets.

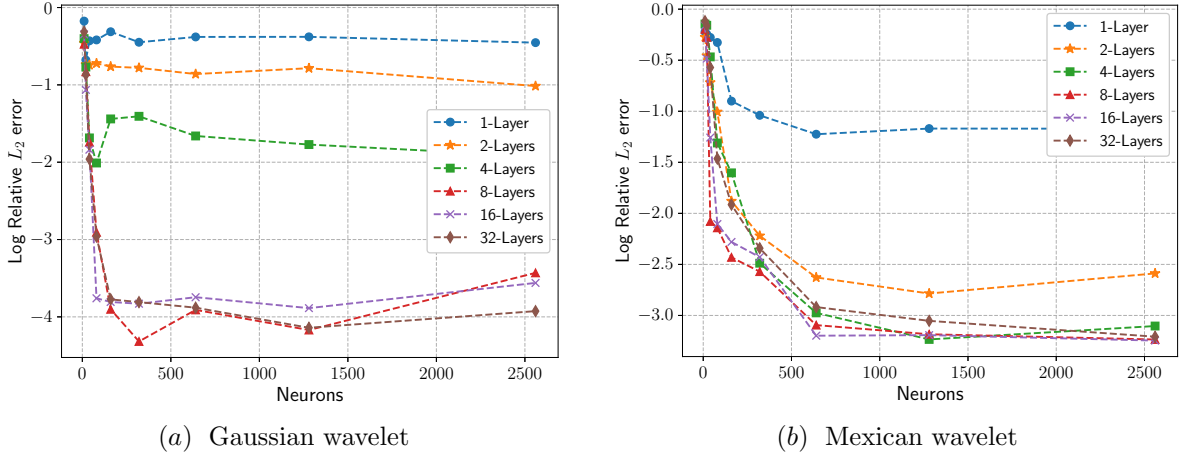


Figure 6: Impact of various hidden layers and number of neurons per layer on performance of W-PINN using Gaussian wavelet(left) and Mexican Hat wavelet(right).

Figure 6 presents experiments on the trainable part of W-PINN. We employ 10,000 collocation points for both Gaussian and Mexican, with resolutions of $[0, 12]$ and $[0, 11]$, respectively. It implies that a shallow network is incapable of learning the behaviors of the problem, regardless of the number of neurons per layer. However, a network with a significant number of layers and sufficient neurons per layer performs adequately. It is redundant to employ a large number of layers and neurons, which results in an increase in computational cost rather than accuracy.

Example 3. Consider the following singularly perturbed nonlinear problem with Neumann boundary conditions

$$\begin{cases} -\epsilon \frac{d^2 u}{dt^2} + u^5 + 3u - 1 = 0, & t \in [0, 1], \\ u'(0) = \sin(0.5), & u'(1) = \exp(-0.7). \end{cases} \quad (8)$$

This example corresponds to a singularly perturbed nonlinear problem with Neumann boundary conditions. This problem possesses boundary layer singularity at both ends. The exact solution to this problem is unknown, so we obtained a numerical solution using Scipy solver and treated it as an exact solution.

Table 6 represents the parameters of the network for the Example 3. The results have been displayed in Table 7 and Figure 7. Specifically, the Table 7 compares the performance of W-PINN, traditional PINN, and the PINN with gaussian wavelet as activation function [34] for various ϵ in terms of relative L_2 -error and average training time. From this table, it is evident that W-PINN takes much less training time and approximates the solution to a better extent. Figure 7 demonstrates as the singularity becomes more

Table 6: Parameters used for Example 3.

| Parameters | Value |
|----------------------------------|---------------|
| Set of resolutions (J_M/J_G) | $[0,8]/[0,9]$ |
| Number of hidden layers | 8 |
| Neurons per layer | 200 |
| Number of collocation points | 10^4 |
| Maximum number of iterations | 10^4 |

Table 7: Performance comparison of various methods for Example 3

| ϵ | Method | L_2 -error | Average Training Time |
|----------------------|-------------------------|--------------|-----------------------|
| $\epsilon = 2^{-4}$ | PINN | 8.6e-05 | 2m 26s |
| | Wavelet Activation [34] | 3.2e-04 | 4m 49s |
| | W-PINN (Gaussian) | 4.7e-05 | 28s |
| | W-PINN (Mexican hat) | 1.4e-04 | 34s |
| $\epsilon = 2^{-7}$ | PINN | 1.8e-03 | 4m 41s |
| | Wavelet Activation [34] | 4.1e-03 | 6m 13s |
| | W-PINN (Gaussian) | 8.9e-06 | 14s |
| | W-PINN (Mexican hat) | 8.3e-05 | 21s |
| $\epsilon = 2^{-10}$ | PINN | 5.3e-03 | 7m 14s |
| | Wavelet Activation [34] | 8.4e-03 | 12m 28s |
| | W-PINN (Gaussian) | 6.5e-06 | 13s |
| | W-PINN (Mexican hat) | 9.9e-05 | 28s |

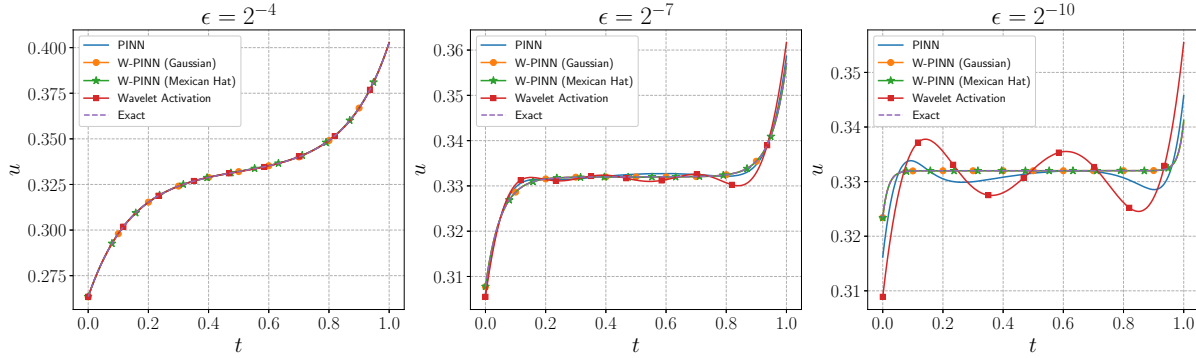


Figure 7: Comparison of solutions obtained by PINN, PINN with wavelet activation and W-PINN methods for Example 3.

prominent, W-PINN effectively addresses the singularity to a greater degree at both ends, in contrast, both PINNs method couldn't resolve singularity and introduce unnatural oscillations over the domain.

Example 4. *FitzHugh-Nagumo (FHN) model* [43]:

The FitzHugh-Nagumo (FHN) model is a simplified version of the Hodgkin-Huxley model, which simulates the dynamics of spiking neurons. It captures the core aspects of how a neuron generates electrical signals (spikes) in response to stimulation (an external current). The mathematical form of the FHN dynamical model is defined as follows:

$$\begin{cases} \frac{dv}{dt} - v + \frac{v^3}{3} + w - RI = 0, \\ \tau \frac{dw}{dt} - v + bw + a = 0, \end{cases} \quad (9)$$

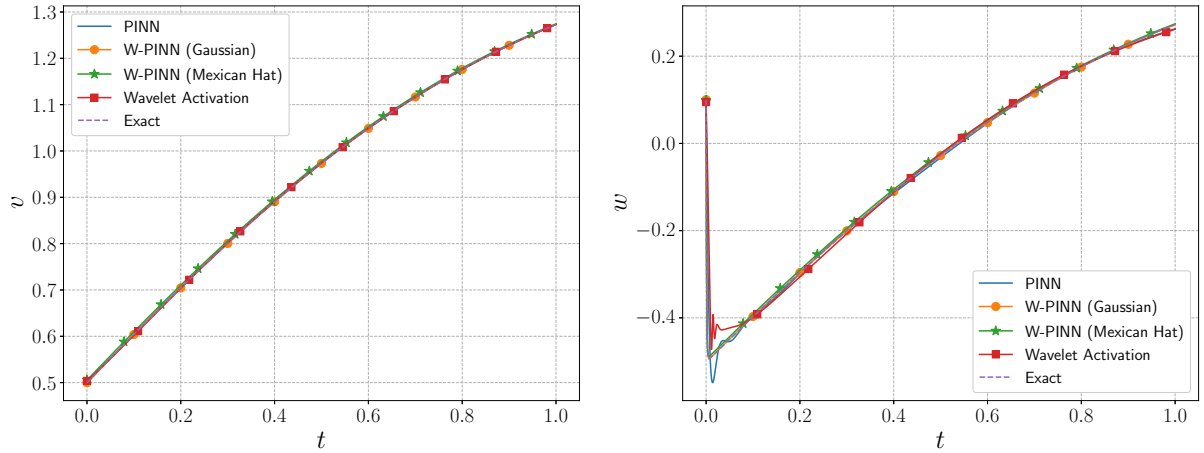
where v denotes the membrane voltage of the neuron, w is the recovery variable, reflecting the activation state of ion channels, I represents the external current applied to the neuron, and R is the resistance across the neuron. In addition, a and b are scaling parameters, and τ denotes the time constant for

Table 8: Parameters used for Example 4.

| Parameters | Value |
|----------------------------------|-----------------|
| Set of resolutions (J_M/J_G) | $[0,10]/[0,11]$ |
| Number of hidden layers | 10 |
| Neurons per layer | 200 |
| Number of collocation points | 10^4 |
| Number of iterations | 2×10^4 |

Table 9: Comparison of various methods for Example 4 with $\tau = 0.15$.

| Methods | L_2 -error (v/w) | Average Training Time |
|----------------------|----------------------------|--------------------------|
| PINN | $5.9e - 04$ $8.1e - 02$ | 6m 38s |
| Wavelet Activation | $2.1e - 03$ 0.11 | 8m 22s |
| W-PINN (Gaussian) | $9.2e - 05$ $5.7e - 04$ | 1m 06s |
| W-PINN (Mexican hat) | $4.4e - 03$ $8.2e - 03$ | 1m 36s |

Figure 8: Comparison of solution of FHN model 4 obtained by PINN, PINN with wavelet activation and W-PINN methods using $\tau = 2^{-10}$.

the recovery variable (w), which acts as a singularly perturbed parameter for this model. In particular, $a = b = 0$, the FHN model describes the Van der Pol oscillator, which describes self-sustaining oscillations in many systems, such as heartbeats, economies, and electronic circuits.

For the numerical computations, we set: $a = 1$, $b = 1$, $I = 0.1$, $R = 1$, and $\tau = 2^{-10}$, $v(0) = 0.5$ and $w(0) = 0.1$. The dynamics of the system are computed till $t = 1$. Table 8 provides the parameters for this Example 4. From Table 9, it is evident that W-PINN gets a more accurate prediction and

Table 10: Parameters used for Example 5.

| Parameters | Value |
|---------------------------------|------------------|
| Set of resolutions (J_x, J_t) | $[-3,5], [-3,5]$ |
| Number of hidden layers | 6 |
| Neurons per layer | 50 |
| Number of collocation points | 10^4 |
| Number of boundary points | 10^3 |
| Number of initial points | 500 |

takes significantly less training time. Figure 8 compares the W-PINN approximations of v and w with PINN and PINN with wavelet activation. The figure illustrates that a strong initial layer is present in the solution profile of w , that both PINN fail to capture and generate spurious oscillations near the singularity, whereas W-PINN effectively resolves the singularity.

Example 5. *A heat conduction problem with large gradients [44]:*

The heat conduction problem investigates temperature flow when an intense heat source suddenly appears. It represents a practical challenge often seen in fusion applications, where researchers need to understand and model rapid heat transfer.

The following mathematical model includes a small positive constant ϵ that creates steep temperature gradients, making it a useful test case for our developed method:

$$\begin{cases} \frac{du}{dt} = \frac{d^2u}{dx^2} + f(x, t), & x \in (-1, 1), t \in [0, 1], \\ u(x, 0) = (1 - x^2) \exp\left(\frac{1}{1 + \epsilon}\right), & x \in (-1, 1), \\ u(-1, t) = 0, u(1, t) = 0, & t \in (0, 1], \end{cases} \quad (10)$$

where f is chosen such that $u(x, t) = (1 - x^2) \exp\left(\frac{1}{(2t - 1)^2 + \epsilon}\right)$ is the exact solution.

The behavior of this model exhibits interesting characteristics depending on the value of the parameter ϵ . When ϵ is relatively large, the solution u demonstrates smooth variations across the computational domain. However, when ϵ becomes very small, the solution shows dramatic changes near $t = 0.5$, exhibiting distinct multi-scale characteristics. An important observation is the relationship between the supervised loss term and the residual term - while the boundary conditions ensure the supervised loss term remains minimal (as the boundary value is 0 and initial value stays below ϵ), the residual term grows considerably as ϵ decreases. This is quantitatively demonstrated as, when $\epsilon = 0.15$ the ratio of $\mathcal{L}_{bc} : \mathcal{L}_{ic} : \mathcal{L}_{res} = 1 : 10 : 10^7$. Traditional PINN methods generally perform well for smooth problems,

Table 11: Comparison of various methods for Example 5 with $\epsilon = 0.15$.

| Methods | L_2 -error | Average Training Time |
|--------------------------|--------------------------------|-----------------------|
| Conventional PINN | $1.07 \pm 0.11 \times 10^0$ | - |
| SA-PINN [24] | 1.76×10^{-3} | 66.75 min |
| MMPINN-DNN [23] | $5.01 \pm 1.52 \times 10^{-4}$ | 11.02 min |
| W-PINN (proposed method) | $3.96 \pm 1.3 \times 10^{-4}$ | 9.5 min |

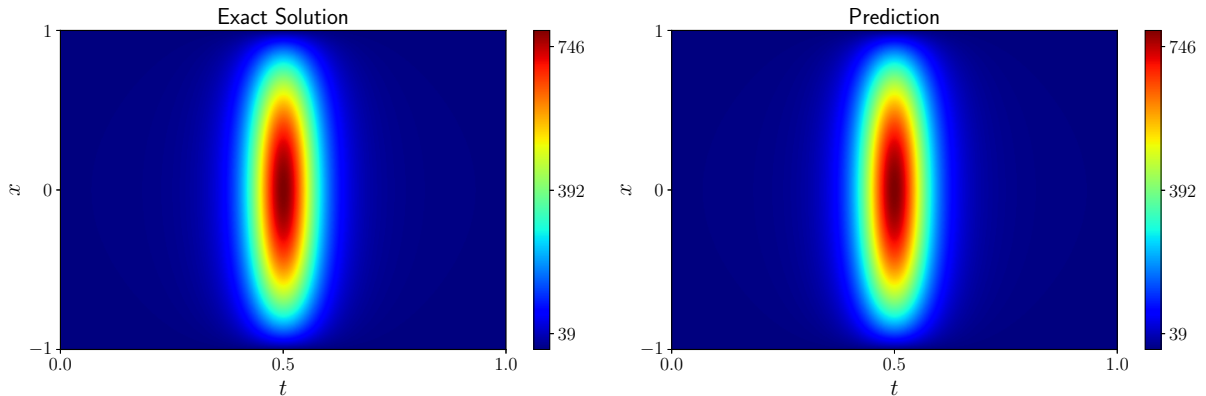


Figure 9: The exact solution (left) and the prediction of W-PINN (right) with $\epsilon = 0.15$ for Example 5 .

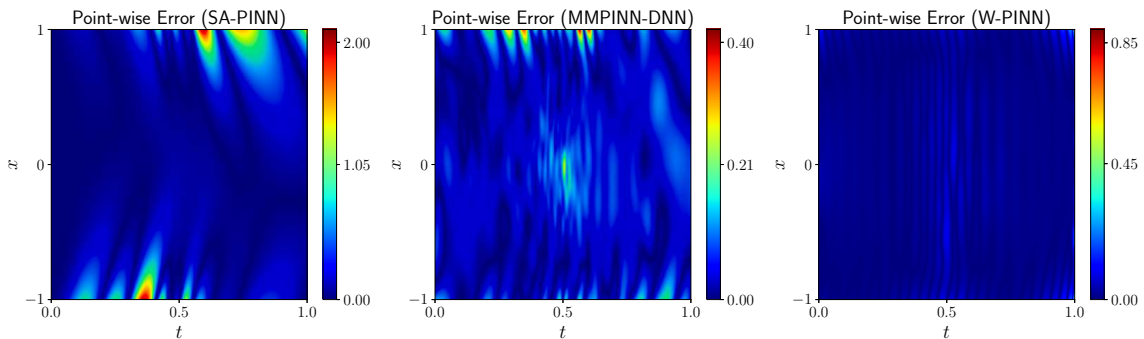
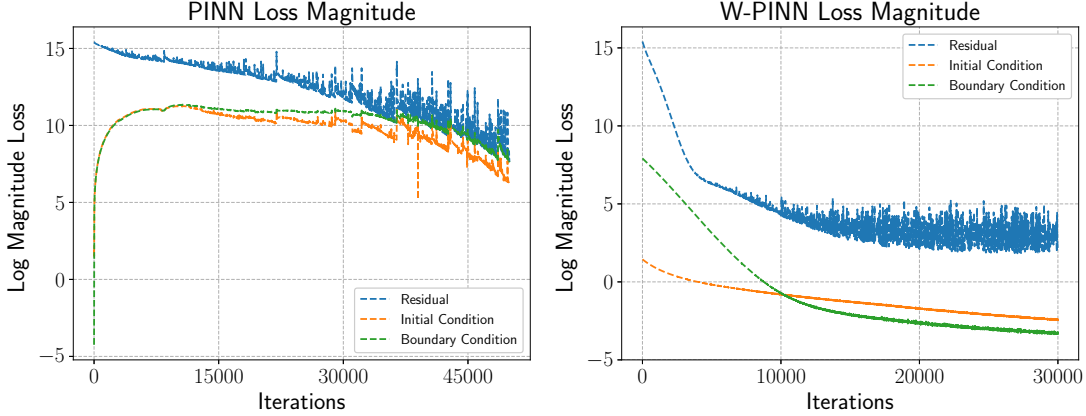


Figure 10: Point-wise absolute error for Example 5. From left to right: SA-PINN, MMPINN-DNN, and W-PINN.

but face challenges when dealing with such large disparities between supervised and residual terms. Our proposed W-PINN can effectively handle such loss imbalances.

Table 10 represents the parameters of the network for this Example 5. Further, Table 11 presents a comparative analysis of different methods for solving Example 5 with $\epsilon = 0.15$, evaluating them based on L_2 -error and average training time. The conventional PINN fails to get an accurate prediction. The SA-PINN [24] shows significant improvement in accuracy but requires substantial computational resources, as evident from its lengthy training time. The MMPINN-DNN [23] achieves better accuracy with reduced computational cost. However, our proposed W-PINN approach demonstrates the most promising balance between accuracy and efficiency. It achieves comparable or better accuracy than other advanced methods while reducing the computational overhead, making it particularly attractive for practical applications. This improvement in both accuracy and computational efficiency highlights the effectiveness of our proposed W-PINN in handling multi-scale characteristics.

Figure 9 demonstrates the similarity between the exact solution and the W-PINN's prediction for Example 5. Figure 10 shows point-wise absolute error comparisons across three different approaches: SA-PINN, MMPINN-DNN, and W-PINN. This error plot shows that errors for W-PINN throughout the domain remain consistently low except for extremely small regions near corners. Further, Figure 11 demonstrates the training progress of conventional PINN and W-PINN by showing their loss components over iterations. PINN shows unstable behavior with the boundary and initial condition losses initially increasing, suggesting potential training difficulties. In contrast, W-PINN exhibits a much more stable and efficient training pattern, where all three loss components (residual, initial condition, and boundary condition) consistently decrease from the start, reaching lower magnitudes in fewer iterations. This

Figure 11: Loss curve of PINN (left) and W-PINN (right) for Example 5 with $\epsilon = 0.15$.

indicates that W-PINN achieves better optimization performance than the standard PINN approach.

Example 6. *Helmholtz equation with high-frequency:*

The Helmholtz equation is a crucial elliptic partial differential equation that models electromagnetic wave behavior. It appears in wide applications in physics and engineering. The equation combines the Laplacian operator (Δu) with a wave number term (c^2), and is typically studied on bounded domains with appropriate boundary conditions. In the high-frequency regime, this equation becomes particularly challenging to solve numerically due to the oscillatory nature of its solutions.

$$\begin{cases} \Delta u(x, y) + c^2 u(x, y) = f(x, y), & (x, y) \in \Omega = (-1, 1) \times (-1, 1), \\ u(x, y) = p(x, y), & (x, y) \in \partial\Omega. \end{cases} \quad (11)$$

f and p are obtained in such a way $u(x, y) = \sin(b_1 \pi x) \sin(b_2 \pi y)$ is the exact solution.

Due to the significant initial imbalance between residual and supervised components, conventional PINN fails to provide accurate predictions as the optimization process becomes heavily skewed towards residual minimization [45].

To test the performance of W-PINN, we set the model parameters as $c = 1$, $b_1 = 1$, and $b_2 = 8$. Table 12 represents the parameters of the network for this Example 6. The comparative analysis presented in Table 13 demonstrates that W-PINN achieves comparable or superior accuracy in terms of L_2 -error relative to state-of-the-art methods in recent literature. Along with its significantly reduced training time, W-PINN is established as a particularly attractive framework. Figure 12 illustrates the remarkable agreement between the analytical solution and W-PINN predictions across the entire domain. In Figure 13, cross-sectional comparisons at various x -coordinates further validate the method's accuracy, with predicted solutions being indistinguishable from the exact solutions.

Table 12: Parameters used for Example 6.

| Parameters | Value |
|-----------------------------------|--------------------|
| Set of resolutions (J_x, J_t) | $[-4, 5], [-4, 5]$ |
| Number of hidden layers | 6 |
| Neurons per layer | 50 |
| Number of collocation points | 10^4 |
| Number of boundary points | 10^3 |

Table 13: Comparison of various methods for Example 6.

| Methods | L_2 -error | Average Training Time |
|--------------------------|--------------------------------|-----------------------|
| Conventional PINN | $4.93 \pm 1.56 \times 10^{-2}$ | 23.18 min |
| SA-PINN [24] | $1.27 \pm 1.11 \times 10^{-2}$ | 152.88 min |
| MMPINN-MFF[23] | $6.56 \pm 4.17 \times 10^{-4}$ | 22.75 min |
| MMPINN-INN[23] | $2.13 \pm 0.43 \times 10^{-4}$ | 64.29 min |
| W-PINN (proposed method) | $3.12 \pm 0.71 \times 10^{-4}$ | 6.3 min |

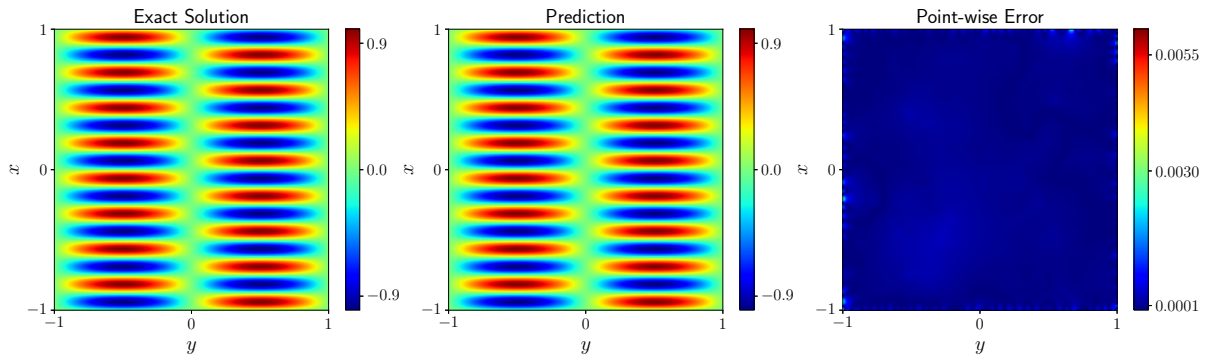


Figure 12: From left to right: The exact solution, the predicted solution, and the Point-wise Error using W-PINN for the Helmholtz equation 6

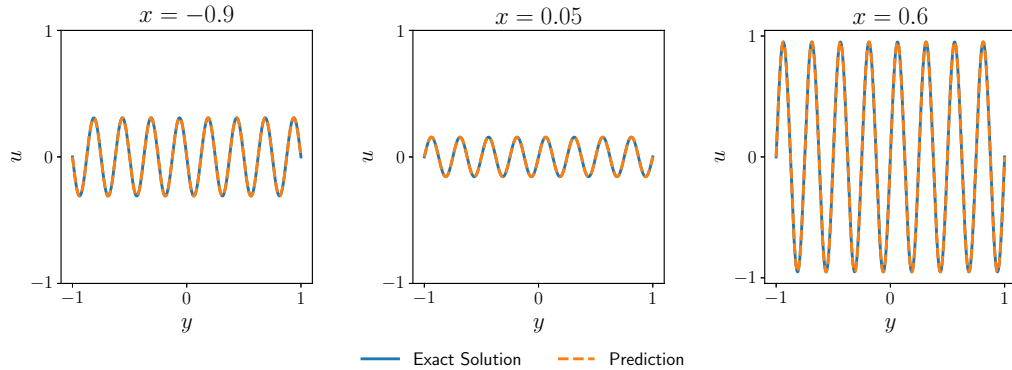


Figure 13: Comparison of the exact solution and the prediction using W-PINN for Example 6.

Example 7. Allen-Cahn reaction-diffusion equation:

The Allen-Cahn reaction-diffusion PDE is a widely used model in materials science, particularly for simulating phase separation processes in metallic alloys [46, 47]. The equation describes the evolution of an order parameter, u , which represents the phase state of the material. The PDE combines a diffusion term, with a nonlinear reaction term that drives the phase separation. The Allen-Cahn equation used in

Table 14: Parameters used for Example 7.

| Parameters | Value |
|------------------------------|------------------|
| Resolutions (J_x, J_t) | $[-5,6], [-5,5]$ |
| Number of hidden layers | 6 |
| Neurons per layer | 100 |
| Number of collocation points | 2×10^4 |
| Number of boundary points | 2×10^3 |
| Number of initial points | 10^3 |

Table 15: Comparison of various methods for Example 7 with $\epsilon = 10^{-4}$.

| Methods | L_2 -error |
|-----------------------------|--|
| Conventional PINN | 0.96 ± 0.06 |
| Time-adaptive approach [48] | $8.0 \times 10^{-2} \pm 0.56 \times 10^{-2}$ |
| SA-PINN [24] | $2.1 \times 10^{-2} \pm 1.21 \times 10^{-2}$ |
| W-PINN (proposed method) | $4.8 \times 10^{-2} \pm 0.6 \times 10^{-2}$ |

this study is defined as:

$$\begin{cases} u_t - \epsilon u_{xx} + 5u^3 - 5u = 0, & x \in [-1, 1], \quad t \in [0, 1], \\ u(t, -1) = u(t, 1), \\ u_x(t, -1) = u_x(t, 1), \\ u(x, 0) = x^2 \cos(\pi x), \end{cases} \quad (12)$$

here ϵ denotes a singularly perturbed parameter. For numerical computations, we choose $\epsilon = 10^{-4}$. Moreover, the exact solution to this problem is unknown, so we obtained a numerical solution using Scipy solver and treated it as an exact solution. The Allen-Cahn equation is particularly challenging due to its rapid changes across space and time, making it difficult to model accurately. Additionally, its periodic boundary conditions provide an extra layer of complexity, making it an ideal benchmark for testing the model's capabilities.

Table 15 presents a comparative analysis of different PINN-based methods. The conventional PINN completely fails to capture the complex dynamics of the problem. While the time-adaptive method [48] shows some improvement, its accuracy remains unsatisfactory. In contrast, our proposed W-PINN achieves accuracy comparable to SA-PINN [24] while demonstrating computational efficiency with approximately twice the speed (30 ms/iteration) of SA-PINN. Figure 14 illustrates the predicted dynamics using the W-PINN method, where the predominance of dark blue regions in the error distribution plot indicates consistently low prediction errors across the solution domain. Further, Figure 15 presents a comparison of W-PINN prediction with the exact solution at three different time stamps, validating the model's ability to accurately capture the temporal evolution of the system dynamics.

Example 8. Maxwell's Equation:

Maxwell's equations represent the fundamental principles governing electromagnetic theory, describing the relationships between electric and magnetic fields and their interaction with matter. Their applications span numerous fields of engineering and physics. In telecommunications, these equations govern the

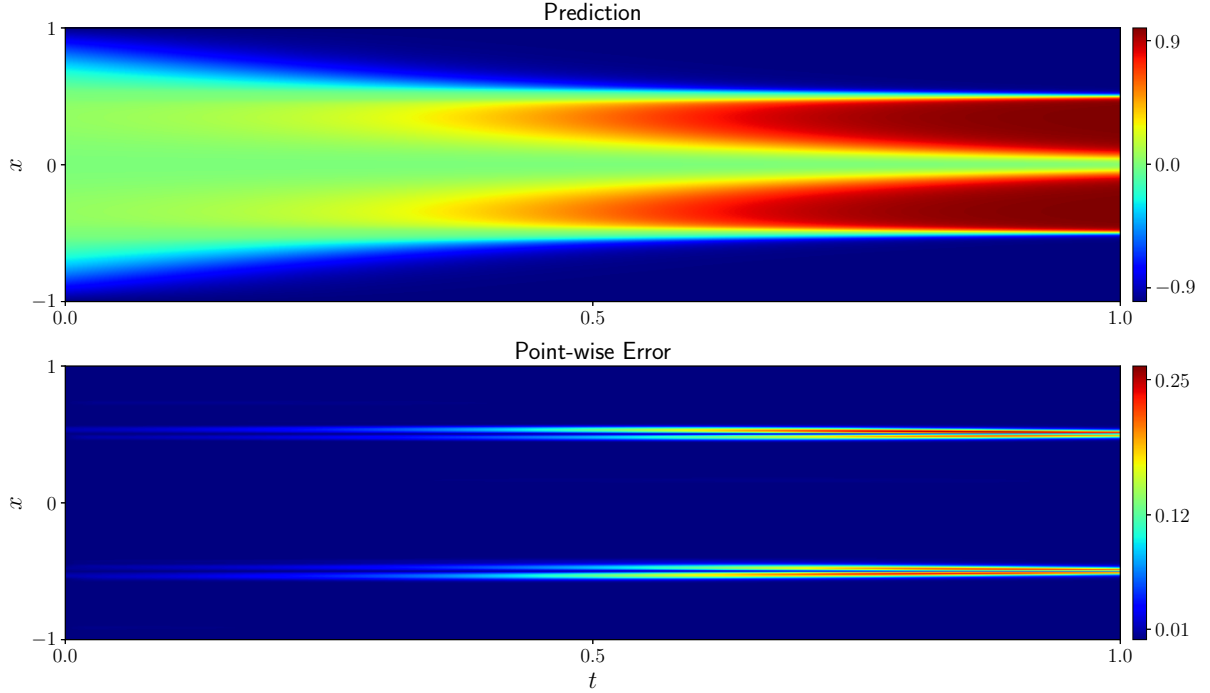


Figure 14: Top: Predicted solution of Allen-Cahn equation 7 via W-PINN. Bottom: point-wise absolute error distribution.

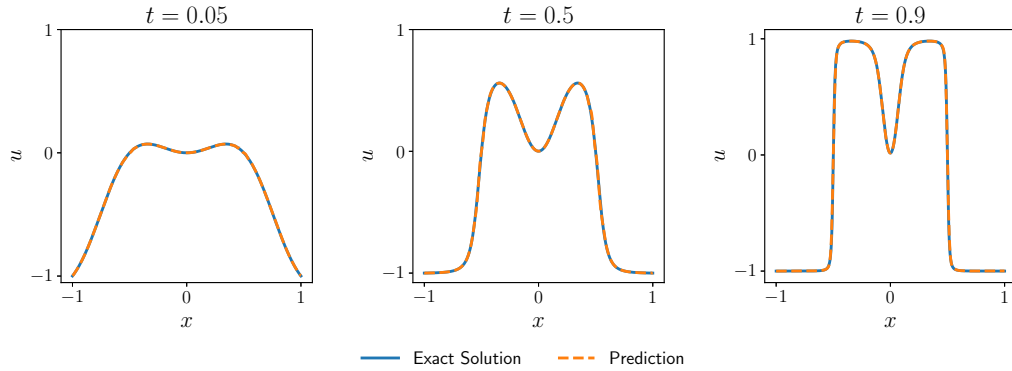


Figure 15: Comparison between exact solution (solid blue line) and predicted solution (dashed orange line) at different time instances for Example 7.

propagation of electromagnetic waves through optical fibers and wireless channels. The medical industry relies heavily on Maxwell's equations for diagnostic imaging technologies, particularly in magnetic resonance imaging (MRI) [49]. In the aerospace sector, these equations are essential for radar system design and satellite communication systems. In their differential form, Maxwell's equations are expressed as:

$$\begin{cases} \nabla \times \mathbf{E}(t, \mathbf{x}) = -\mu(\mathbf{x}) \frac{\partial \mathbf{H}(t, \mathbf{x})}{\partial t}, \\ \nabla \times \mathbf{H}(t, \mathbf{x}) = \varepsilon(\mathbf{x}) \frac{\partial \mathbf{E}(t, \mathbf{x})}{\partial t}, \end{cases} \quad (13)$$

where \mathbf{E} is the electric field vector, \mathbf{H} is the magnetic field vector. The material properties are

Table 16: Parameters used for Example 8.

| Parameters | Value |
|------------------------------|------------------|
| Resolutions (J_x, J_t) | $[-5,5], [-5,5]$ |
| Number of hidden layers | 6 |
| Neurons per layer | 50 |
| Number of collocation points | 10^4 |
| Number of boundary points | 500 |
| Number of initial points | 500 |

characterized by μ , the magnetic permeability, which quantifies the medium's response to magnetic fields, and ϵ , the electric permittivity, which describes the medium's capacity to store electrical energy. The operators ∇ and \times represent the del operator and cross product, respectively.

A significant challenge in solving these equations arises from their inherent rapid oscillations in both space and time. This characteristic poses particular difficulties for traditional PINNs, especially when dealing with heterogeneous media where μ and ϵ exhibit discontinuous behavior at media interfaces. Here, we present a solution of Maxwell's equation in both a homogeneous and a heterogeneous medium via W-PINN and compare them with the traditional PINN.

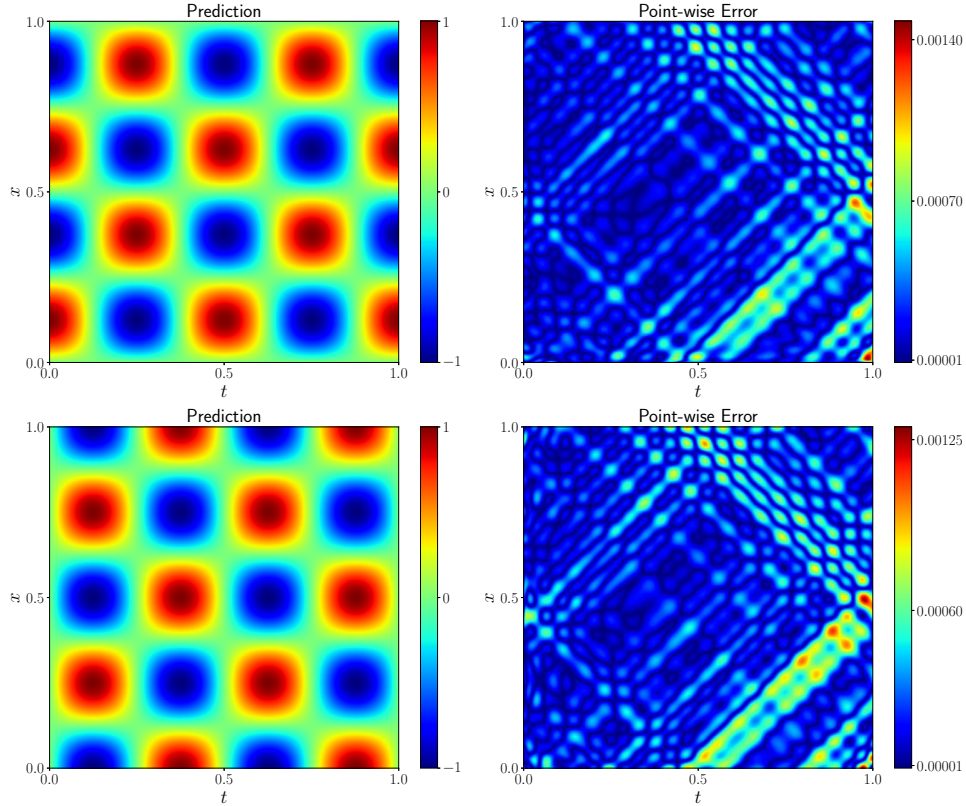


Figure 16: Top: E_y predicted at the left and corresponding point-wise error at the right. Bottom: H_z predicted and corresponding point-wise error for the Maxwell's equation14 in homogeneous media via W-PINN.

A. Homogeneous media

We first investigate the performance of our proposed method by solving Maxwell's equations in a one-dimensional cavity model with homogeneous media. The governing equations are:

$$\frac{\partial E_y}{\partial t} = -\frac{1}{\epsilon} \frac{\partial H_z}{\partial x}, \quad \frac{\partial H_z}{\partial t} = -\frac{1}{\mu} \frac{\partial E_y}{\partial x}, \quad x \in [0, 1], \quad t \in [0, 1]. \quad (14)$$

The system is subject to perfectly electric conductor (PEC) boundary conditions:

$$\begin{cases} E_y(0, t) = E_y(1, t) = 0, \\ \left. \frac{\partial H_z(x, t)}{\partial x} \right|_{x=0,1} = 0. \end{cases} \quad (15)$$

The ground truth for the example is given by:

$$\begin{cases} E_y = \sin(n\pi x) \cos(\omega t), \\ H_z = -\cos(n\pi x) \sin(\omega t), \end{cases} \quad (16)$$

where $n = 4$ is the order of cavity mode, cavity frequency $\omega = n\pi/l$ and l is the length of medium.

Over five random runs, W-PINN achieved average relative L2-errors of $5.74 \pm 2.12 \times 10^{-4}$ and $6.11 \pm 3.01 \times 10^{-4}$ for E_y and H_z , respectively. In contrast, traditional PINNs exhibited notably higher errors

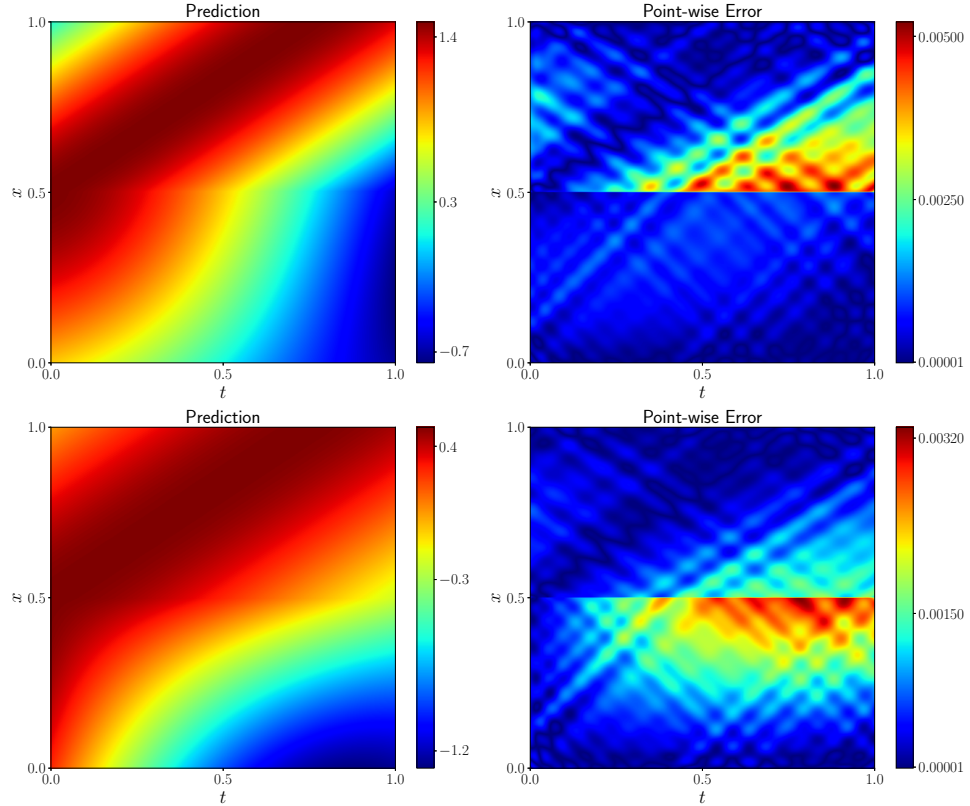


Figure 17: Top: E_y predicted at the left and corresponding point-wise error at the right. Bottom: H_z predicted and corresponding point-wise error for the Maxwell's equation 14 in heterogeneous media via W-PINN.

of $3.08 \pm 1.18 \times 10^{-3}$ and $5.18 \pm 1.93 \times 10^{-3}$. The computational efficiency of W-PINN is evident in its training time, requiring an average of 4.2 minutes with 18 ms per iteration on Nvidia A6000 GPU. The network architecture parameters are tabulated in Table 16. Figure 16 presents the W-PINN predictions for both electric and magnetic fields, alongside their corresponding point-wise errors within the cavity. The remarkably low point-wise error distribution validates the high accuracy of our approach in capturing the electromagnetic field behavior.

B. Heterogeneous media

For this case, we chose the Maxwell's equation 14 in a heterogeneous medium with the following analytical solution:

$$E_y = \begin{cases} \cos(2t - 2x + 1) \\ +0.5 \cos(2t + 2x - 1), & \text{if } x \in \Omega_1, \\ 1.5 \cos(2t - 3x + 1.5), & \text{if } x \in \Omega_2, \end{cases} \quad (17)$$

$$H_z = \begin{cases} \cos(2t - 2x + 1) \\ -0.5 \cos(2t + 2x - 1), & \text{if } x \in \Omega_1, \\ 0.5 \cos(2t - 3x + 1.5), & \text{if } x \in \Omega_2, \end{cases} \quad (18)$$

where $\Omega_1 = [0, 0.5]$ and $\Omega_2 = [0.5, 1]$. Here $\mu = 1, \epsilon = 1$ in Ω_1 and $\mu = 4.5, \epsilon = 0.5$ in Ω_2 . According to electromagnetic interface condition:

$$\begin{cases} E_y(0.5, t)|_{x \in \Omega_1} = E_y(0.5, t)|_{x \in \Omega_2}, \\ H_z(0.5, t)|_{x \in \Omega_1} = H_z(0.5, t)|_{x \in \Omega_2}. \end{cases} \quad (19)$$

In this challenging context of heterogeneous media, W-PINN demonstrates remarkable accuracy, achieving average relative L2-errors of $2.41 \pm 1.22 \times 10^{-4}$ and $2.81 \pm 1.51 \times 10^{-4}$ for electric (E_y) and magnetic (H_z) fields, respectively. These results represent a two-order-of-magnitude improvement over traditional PINNs, which exhibit substantially higher errors of $1.37 \pm 1.18 \times 10^{-2}$ and $2.07 \pm 0.51 \times 10^{-2}$. W-PINN took an average of 6.1 minutes with around 30 ms/iteration on Nvidia A6000 GPU. The network parameters are the same as in Table 16. Figure 17 illustrates the W-PINN predictions for both electric and magnetic fields, alongside their corresponding point-wise errors. While the media interface presents the greatest computational challenge (point-wise error regions in red), W-PINN maintains impressive accuracy throughout the domain, successfully capturing the Electromagnetic field behavior across the media.

Example 9. Lid-Driven Cavity flow:

The steady two-dimensional incompressible lid-driven cavity flow is a classic benchmark problem in computational fluid dynamics. The flow is governed by the incompressible Navier-Stokes equations, which present significant challenges due to their nonlinear nature and the presence of pressure-velocity coupling. As illustrated in Figure 18, the problem consists of a unit square cavity where the top wall moves with a uniform velocity of 1 unit while maintaining no-slip conditions on all other walls. The governing Navier-Stokes equations for this system are:

$$\begin{cases} \frac{\partial u}{\partial x} + \frac{\partial v}{\partial y} = 0, \\ u \frac{\partial u}{\partial x} + v \frac{\partial u}{\partial y} + \frac{\partial p}{\partial x} - \frac{1}{\text{Re}} \left(\frac{\partial^2 u}{\partial x^2} + \frac{\partial^2 u}{\partial y^2} \right) = 0, \\ u \frac{\partial v}{\partial x} + v \frac{\partial v}{\partial y} + \frac{\partial p}{\partial y} - \frac{1}{\text{Re}} \left(\frac{\partial^2 v}{\partial x^2} + \frac{\partial^2 v}{\partial y^2} \right) = 0, \end{cases} \quad (20)$$

Table 17: Parameters used for Example 9.

| Parameters | Value |
|------------------------------|--------------------|
| Resolutions (J_x, J_t) | $[-10,5], [-10,5]$ |
| Number of hidden layers | 10 |
| Neurons per layer | 80 |
| Number of collocation points | 2×10^4 |
| Number of boundary points | 1000 |

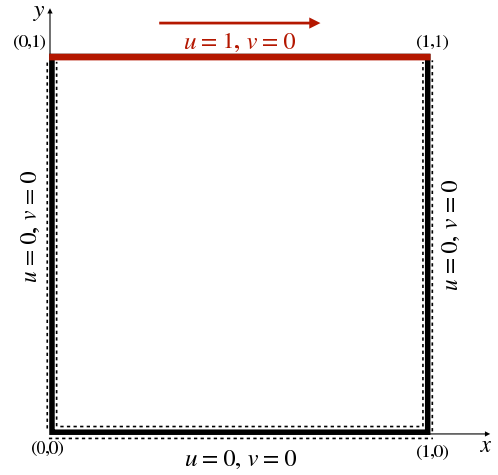
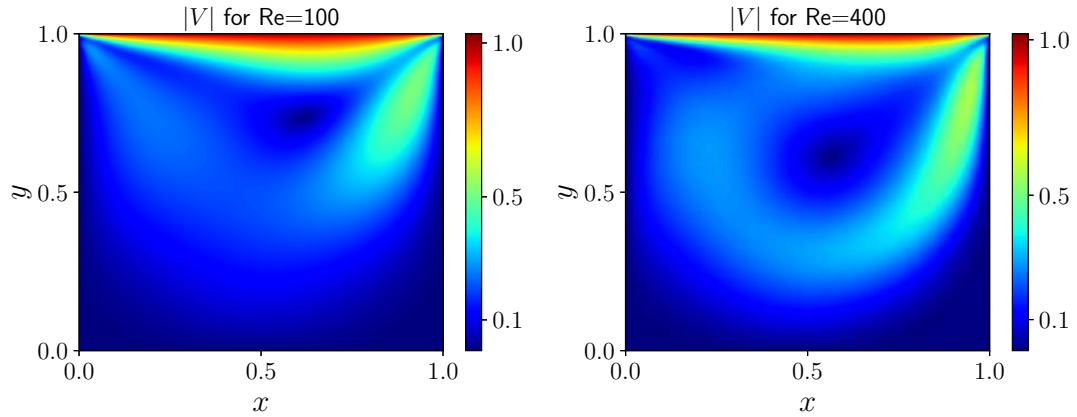
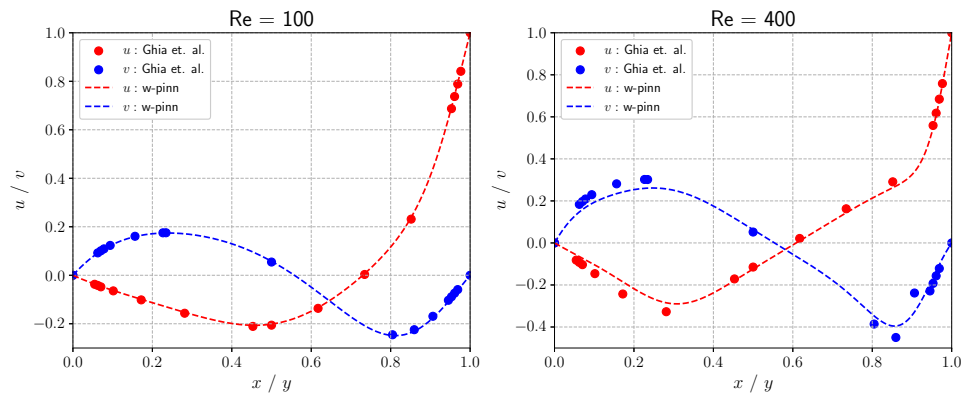


Figure 18: A lid-driven unit square cavity.

Figure 19: Predicted fluid speed for the steady-state lid-driven cavity flow 20 for $Re=100$ (left) and $Re=400$ (right) via W-PINN.Figure 20: Comparison of W-PINN solution (dashed line) with Ghia's benchmark (scattered circles) for the steady-state lid-driven cavity flow 20 for $Re=100$ (left) and $Re=400$ (right).

where u and v are the fluid velocities in x and y directions respectively, and p is the fluid pressure. Re is Reynolds number which represents the ratio of inertial forces to viscous forces. We evaluate our W-PINN approach for two distinct flow regimes: $Re = 100$ and $Re = 400$, comparing our results against the widely-accepted benchmark solutions of Ghia et al.[50].

For this example, network's parameters are tabulated in 17. Figure 19 presents the fluid flow speed distribution ($|V| = \sqrt{u^2 + v^2}$) predicted by W-PINN, demonstrating successful capture of the characteristic vortex structure. Quantitative validation against Ghia's benchmark data is illustrated in Figure 20. For $Re = 100$, the maximum absolute errors are 3.41×10^{-3} and 2.46×10^{-3} for u and v components respectively. At the higher Reynolds number of 400, where flow complexity increases, the errors remain within acceptable bounds at 4.79×10^{-2} and 6.69×10^{-2} . These results demonstrate W-PINN's robust capability in handling complex fluid dynamics problems to a good extent.

4. Conclusion

An efficient W-PINN for singularly perturbed problems is developed. This study successfully demonstrated the advantages of W-PINNs over other PINN-based methods in dealing with problems with steep gradients, rapid oscillations, and singular or multiscale behavior. The wavelet theory served as the foundation for the development of W-PINN, which combined the learning efficiency of PINN with the localization properties of wavelets (both in scale and space) to capture nonlinear information within localized regions. A limitation of the proposed method is that the number of required basis functions grows exponentially with dimension, leading to computational challenges for high-dimensional PDEs. Investigating dimensionality reduction or sparse representation techniques can address this limitation in future research. In addition to this, W-PINNs could prove effective for other problems that exhibit singular behavior, such as fractional differential models, which inherently possess such characteristics.

CRedit authorship contribution statement

Himanshu Pandey: Conceptualization, Methodology, Programming, Formal analysis, Writing - original draft. **Anshima Singh:** Conceptualization, Investigation, Methodology, Formal analysis, Writing - original draft. **Ratikanta Behera:** Funding acquisition, Supervision, Writing - review & editing.

Declaration of competing interest

The authors declare that there are no conflicts of interest.

Data Availability Statement

No data was used for the research described in the article.

Acknowledgments

Ratikanta Behera is supported by the Anusandhan National Research Foundation (ANRF), Government of India, under Grant No. EEQ/2022/001065. We would like to express our gratitude to the Editor for taking time to handle the manuscript and to anonymous referees whose constructive comments are very helpful for improving the quality of our paper.

Preprint

A preprint of this paper is available on arxiv with Ref. No. arXiv:2409.11847

References

- [1] H.-G. Roos, M. Stynes, L. Tobiska, Robust numerical methods for singularly perturbed differential equations, 2nd Edition, Vol. 24 of Springer Series in Computational Mathematics, Springer-Verlag, Berlin, 2008, convection-diffusion-reaction and flow problems. doi:10.1007/978-3-540-34467-4.
- [2] W. O. Criminale, T. L. Jackson, D. G. Lasseigne, R. D. Joslin, Perturbation dynamics in viscous channel flows, *J. Fluid Mech.* 339 (1997) 55–75. doi:10.1017/S0022112097005235.
- [3] R. M. Turian, Solutions of problems in chemical flow reactors by perturbation methods, *Chem. Eng. Sci.* 28 (11) (1973) 2021–2031. doi:10.1016/0009-2509(73)85046-8.
- [4] J.-P. Fouque, G. Papanicolaou, R. Sircar, K. Solna, Singular perturbations in option pricing, *SIAM J. Appl. Math.* 63 (5) (2003) 1648–1665. doi:10.1137/S0036139902401550.
- [5] P. A. Markowich, C. A. Ringhofer, A singularly perturbed boundary value problem modelling a semiconductor device, *SIAM J. Appl. Math.* 44 (2) (1984) 231–256. doi:10.1137/0144018.
- [6] I. Pop, D. B. Ingham, Convective heat transfer: mathematical and computational modelling of viscous fluids and porous media, Elsevier, 2001. doi:10.1016/B978-008043878-8/50021-3.
- [7] D. N. d. G. Allen, R. V. Southwell, Relaxation methods applied to determine the motion, in two dimensions, of a viscous fluid past a fixed cylinder, *Quart. J. Mech. Appl. Math.* 8 (1955) 129–145. doi:10.1093/qjmam/8.2.129.
- [8] B. Kreiss, H.-O. Kreiss, Numerical methods for singular perturbation problems, *SIAM J. Numer. Anal.* 18 (2) (1981) 262–276. doi:10.1137/0718019.
- [9] T. Linß, Layer-adapted meshes for reaction-convection-diffusion problems, Vol. 1985 of Lecture Notes in Mathematics, Springer-Verlag, Berlin, 2010. doi:10.1007/978-3-642-05134-0.
- [10] A. F. Hegarty, J. J. H. Miller, E. O’Riordan, G. I. Shishkin, Special meshes for finite difference approximations to an advection-diffusion equation with parabolic layers, *J. Comput. Phys.* 117 (1) (1995) 47–54. doi:10.1006/jcph.1995.1043.
- [11] J. Saberi-Nadjafi, F. A. Ghassabzade, The numerical solution of the singularly perturbed differential-difference equations based on the meshless method, *Int. J. Appl. Res.* 3 (2) (2014) 116–121. doi:10.14419/ijamr.v3i2.1595.
- [12] J. Wang, Y. Wu, Y. Xu, F. Sun, A dimension-splitting variational multiscale element-free Galerkin method for three-dimensional singularly perturbed convection-diffusion problems, *Comput. Model. Eng. Sci.* (2023) 341–356 doi:10.32604/cmesci.2022.023140.
- [13] M. Kamranian, M. Dehghan, M. Tatari, An adaptive meshless local Petrov-Galerkin method based on a posteriori error estimation for the boundary layer problems, *Appl. Numer. Math.* 111 (2017) 181–196. doi:10.1016/j.apnum.2016.09.007.
- [14] M. Dissanayake, N. Phan-Thien, Neural-network-based approximations for solving partial differential equations, *Commun. Numer. Meth. Eng.* 10 (3) (1994) 195–201. doi:10.1002/cnm.1640100303.
- [15] I. E. Lagaris, A. Likas, D. I. Fotiadis, Artificial neural networks for solving ordinary and partial differential equations, *IEEE Trans. Neural Netw.* 9 (5) (1998) 987–1000. doi:10.1109/72.712178.
- [16] M. Raissi, P. Perdikaris, G. E. Karniadakis, Physics-informed neural networks: a deep learning framework for solving forward and inverse problems involving nonlinear partial differential equations, *J. Comput. Phys.* 378 (2019) 686–707. doi:10.1016/j.jcp.2018.10.045.
- [17] E. Kharazmi, Z. Zhang, G. E. Karniadakis, Variational physics-informed neural networks for solving partial differential equations, arXiv preprint arXiv:1912.00873 (2019). doi:10.48550/arXiv.1912.00873.
- [18] J. Yu, L. Lu, X. Meng, G. E. Karniadakis, Gradient-enhanced physics-informed neural networks for forward and inverse PDE problems, *Comput. Methods Appl. Mech. Engrg.* 393 (2022) Paper No. 114823, 22. doi:10.1016/j.cma.2022.114823.
- [19] A. D. Jagtap, G. E. Karniadakis, Extended physics-informed neural networks (XPINNs): a generalized space-time domain decomposition based deep learning framework for nonlinear partial differential equations, *Commun. Comput. Phys.* 28 (5) (2020) 2002–2041. doi:10.4208/cicp.oa-2020-0164.
- [20] S. Cuomo, V. Schiano Di Cola, F. Giampaolo, G. Rozza, M. Raissi, F. Piccialli, Scientific machine learning through physics-informed neural networks: where we are and what’s next, *J. Sci. Comput.* 92 (3) (2022) Paper No. 88, 62. doi:10.1007/s10915-022-01939-z.
- [21] G. E. Karniadakis, I. G. Kevrekidis, L. Lu, P. Perdikaris, S. Wang, L. Yang, Physics-informed machine learning, *Nat. Rev. Phys.* 3 (6) (2021) 422–440. doi:10.1038/s42254-021-00314-5.
- [22] A. Arzani, K. W. Cassel, R. M. D’Souza, Theory-guided physics-informed neural networks for bound-

- ary layer problems with singular perturbation, *J. Comput. Phys.* 473 (2023) Paper No. 111768, 15. doi:10.1016/j.jcp.2022.111768.
- [23] Y. Wang, Y. Yao, J. Guo, Z. Gao, A practical PINN framework for multi-scale problems with multi-magnitude loss terms, *J. Comput. Phys.* 510 (2024) Paper No. 113112, 19. doi:10.1016/j.jcp.2024.113112. URL <https://doi.org/10.1016/j.jcp.2024.113112>
- [24] L. D. McClenny, U. M. Braga-Neto, Self-adaptive physics-informed neural networks, *J. Comput. Phys.* 474 (2023) Paper No. 111722, 23. doi:10.1016/j.jcp.2022.111722. URL <https://doi.org/10.1016/j.jcp.2022.111722>
- [25] H. Ren, X. Meng, R. Liu, J. Hou, Y. Yu, A class of improved fractional physics informed neural networks, *Neurocomputing* 562 (2023) 126890. doi:10.1016/j.neucom.2023.126890.
- [26] Z. Mao, A. D. Jagtap, G. E. Karniadakis, Physics-informed neural networks for high-speed flows, *Comput. Methods Appl. Mech. Engrg.* 360 (2020) 112789, 26. doi:10.1016/j.cma.2019.112789. URL <https://doi.org/10.1016/j.cma.2019.112789>
- [27] M. A. Nabian, R. J. Gladstone, H. Meidani, Efficient training of physics-informed neural networks via importance sampling, *Comput.-Aided Civ. Infrastruct. Eng.* 36 (8) (2021) 962–977. doi:<https://doi.org/10.1111/mice.12685>.
- [28] V. Kumar, M. Mehra, Wavelet optimized finite difference method using interpolating wavelets for self-adjoint singularly perturbed problems, *J. Comput. Appl. Math.* 230 (2) (2009) 803–812. doi:10.1016/j.cam.2009.01.017.
- [29] N. Kumar, V. Kumar, M. Mehra, Legendre wavelet collocation method for singularly-perturbed problems using operational matrix and Laplace transformation, *ZAMM Z. Angew. Math. Mech.* 105 (2) (2025) Paper No. e202400200. doi:10.1002/zamm.202400200.
- [30] S. G. Mallat, A theory for multiresolution signal decomposition: the wavelet representation, *IEEE Trans. Pattern Anal. Mach. Intell.* 11 (7) (1989) 674–693. doi:10.1137/1.9781611970104.
- [31] I. Daubechies, Ten lectures on wavelets, Vol. 61 of CBMS-NSF Regional Conference Series in Applied Mathematics, Society for Industrial and Applied Mathematics (SIAM), Philadelphia, PA, 1992. doi:10.1137/1.9781611970104.
- [32] R. Behera, M. Mehra, Integration of barotropic vorticity equation over spherical geodesic grid using multilevel adaptive wavelet collocation method, *Appl. Math. Model.* 37 (7) (2013) 5215–5226. doi:10.1016/j.apm.2012.10.027.
- [33] K. Goyal, M. Mehra, An adaptive meshfree spectral graph wavelet method for partial differential equations, *Appl. Numer. Math.* 113 (2017) 168–185. doi:10.1016/j.apnum.2016.11.011.
- [34] Z. Uddin, S. Ganga, R. Asthana, W. Ibrahim, Wavelets based physics informed neural networks to solve non-linear differential equations, *Sci Rep* 13 (1) (2023) 2882. doi:10.1038/s41598-023-29806-3.
- [35] G. Cybenko, Approximation by superpositions of a sigmoidal function, *Math. Control Signals Systems* 2 (4) (1989) 303–314. doi:10.1007/BF02551274.
- [36] D. E. Rumelhart, G. E. Hinton, R. J. Williams, Learning representations by back-propagating errors, *nature* 323 (6088) (1986) 533–536. doi:10.1038/323533a0.
- [37] A. I. M. G. Baydin, B. A. Pearlmutter, A. A. Radul, J. M. Siskind, Automatic differentiation in machine learning: a survey, *J. Mach. Learn. Res.* 18 (2017) Paper No. 153, 43. URL <http://jmlr.org/papers/v18/17-468.html>
- [38] R. Sharma, V. Shankar, Accelerated training of physics-informed neural networks (pinns) using meshless discretizations, *NeurIPS* 35 (2022) 1034–1046. doi:10.48550/arXiv.2205.09332.
- [39] D. P. Kingma, J. Ba, Adam: A method for stochastic optimization, *arXiv preprint arXiv:1412.6980* (2014). doi:10.48550/arXiv.1412.6980.
- [40] X. Glorot, Y. Bengio, Understanding the difficulty of training deep feedforward neural networks, in: Y. W. Teh, M. Titterton (Eds.), *Proceedings of the Thirteenth International Conference on Artificial Intelligence and Statistics*, Vol. 9 of *Proceedings of Machine Learning Research*, PMLR, Chia Laguna Resort, Sardinia, Italy, 2010, pp. 249–256. URL <https://proceedings.mlr.press/v9/glorot10a.html>
- [41] C. M. Bender, S. A. Orszag, *Advanced mathematical methods for scientists and engineers. I*, Springer-Verlag, New York, 1999, asymptotic methods and perturbation theory, Reprint of the 1978 original. doi:10.1007/978-1-4757-3069-2.
- [42] Z. Cen, F. Erdogan, A. Xu, An almost second order uniformly convergent scheme for a singularly perturbed

- initial value problem, *Numer. Algorithms* 67 (2) (2014) 457–476. doi:10.1007/s11075-013-9801-0.
- [43] J. Su, Delayed oscillation phenomena in the FitzHugh Nagumo equation, *J. Differential Equations* 105 (1) (1993) 180–215. doi:10.1006/jdeq.1993.1087.
- [44] K. Lan, Dream fusion in octahedral spherical hohlraum, *Matter Radiat. Extrem.* 7 (5) (2022). doi:https://doi.org/10.1063/5.0103362.
- [45] S. Wang, Y. Teng, P. Perdikaris, Understanding and mitigating gradient flow pathologies in physics-informed neural networks, *SIAM J. Sci. Comput.* 43 (5) (2021) A3055–A3081. doi:10.1137/20M1318043. URL https://doi.org/10.1137/20M1318043
- [46] N. Moelans, B. Blanpain, P. Wollants, An introduction to phase-field modeling of microstructure evolution, *Calphad* 32 (2) (2008) 268–294. doi:https://doi.org/10.1016/j.calphad.2007.11.003.
- [47] C. Kunselman, V. Attari, L. McClenny, U. Braga-Neto, R. Arroyave, Semi-supervised learning approaches to class assignment in ambiguous microstructures, *Acta Mater.* 188 (2020) 49–62. doi:https://doi.org/10.1016/j.actamat.2020.01.046.
- [48] C. L. Wight, J. Zhao, Solving Allen-Cahn and Cahn-Hilliard equations using the adaptive physics informed neural networks, *Commun. Comput. Phys.* 29 (3) (2021) 930–954. doi:10.4208/cicp.oa-2020-0086. URL https://doi.org/10.4208/cicp.oa-2020-0086
- [49] R. W. Brown, Y.-C. N. Cheng, E. M. Haacke, M. R. Thompson, R. Venkatesan, *Magnetic resonance imaging: physical principles and sequence design*, John Wiley & Sons, 2014. doi:10.1002/9781118633953.
- [50] U. Ghia, K. Ghia, C. Shin, High-re solutions for incompressible flow using the navier-stokes equations and a multigrid method, *J. Comput. Phys.* 48 (3) (1982) 387–411. doi:https://doi.org/10.1016/0021-9991(82)90058-4.